JP Journal of Heat and Mass Transfer

https://pphmjopenaccess.com
https://doi.org/10.17654/0973576326014
Volume 39, Number 2, 2026, Pages 255-279
P-ISSN: 0973-5763
E-ISSN: 3049-2556

EFFECT OF MAGNETIC FIELD ON A CASSON NANOFLUID OF MHD THROUGH A SINUSOIDAL CHANNEL

T. S. Suchita[1], S. Senthamilselvi[1] and R. Vijayakumar[2,3]

[1]Department of Mathematics
Vels Institute of Science, Technology and Advanced Studies
Tamil Nadu, India
e-mail: msselvi2305@gmail.com
chiku2712@gmail.com

[2]Mathematics Section, FEAT
Annamalai University
Annamalainagar-608002, India

[3]Department of Mathematics
Periyar Arts College
Cuddalore, Tamil Nadu – 607 001, India
e-mail: rathirath_viji@yahoo.co.in

Received: June 17, 2025; Revised: October 1, 2025; Accepted: January 27, 2026

Keywords and phrases: Casson nanofluid, MHD, slip conditions, thermal radiation, wavy channel.

How to cite this article: T. S. Suchita, S. Senthamilselvi and R. Vijayakumar, Effect of magnetic field on a Casson nanofluid of MHD through a sinusoidal channel, JP Journal of Heat and Mass Transfer 39(2) (2026), 255-279. https://doi.org/10.17654/0973576326014

Published Online: March 10, 2026

Abstract

In this research, we investigate the unsteady magnetohydrodynamic (MHD) flow and heat transfer behavior of a Casson nanofluid through a porous, sinusoidal (wavy) artery channel, under the influence of a perpendicular magnetic field. The study considers blood as a base fluid, enhanced with gold nanoparticles, and models it using Casson fluid characteristics to simulate realistic biological and industrial non-Newtonian behaviors. The analysis incorporates Hall and ion slip effects, thermal radiation, and porous medium properties. A perturbation technique is applied to derive analytical solutions to the governing non-dimensional equations for velocity and temperature fields. Key physical parameters such as Hartmann number, Grashof number, suction parameter, Prandtl number, and time are varied to understand their influence on flow dynamics. The results, presented graphically, reveal that increasing the magnetic field strength (Hartmann number) and the suction parameter results in the suppression of fluid motion and temperature profiles, whereas the Hall and ion slip parameters exhibit contrasting effects on the flow velocities. The study concludes that both thermal and hydrodynamic boundary layers are significantly influenced by the interplay of magnetic, thermal, and porous characteristics, providing insights for biomedical and industrial applications involving complex fluid flows.

1. Introduction

Researchers are increasingly interested in non-Newtonian blood models because they more accurately capture physiological flow behavior in biomedical applications such as microcirculation, catheterized arteries, and targeted thermal therapies. Blood is often modeled as a Casson fluid to represent its yield-stress and shear-thinning behavior, which is important when studying flow in narrow, stenosed or wavy arteries. Recent studies have modeled blood as a Casson nanofluid carrying gold (Au) nanoparticles to investigate thermal transport, entropy generation and clinical applications (e.g., drug delivery and localized hyperthermia), because Au nanoparticles offer favorable biocompatibility and strong thermal response for biomedical use. Hall and ion-slip effects, together with magnetic fields, have been shown

to substantially influence velocity and heat transfer in blood-based nanofluids an important consideration for magnetically assisted therapies and magnetohydrodynamic control in catheterized or stenosed arteries. Khan et al. [1] took into account the second-order slip micropolar Casson nanofluid flow with variable viscosity, thermal conductivity, Brownian diffusion, and thermophoretic diffusion also considered the blood flow as a non-Newtonian Casson micropolar nanofluid past a moving stretching elastic sheet. The first analytical model for radiation-induced convective nanofluid flow was developed by Parasuraman et al. [2]. In a rotating environment with fluctuating wall temperature and concentration, Singh et al. [3] investigated the effects of Hall and ion-slip currents on the unsteady MHD boundary layer flow of electrically and thermally conducting, heat-absorbing, and chemically reacting Walters'B fluid over an infinite vertical porous plate embedded in a uniform porous medium. Singh et al. [4] reported on an analytical study on an unsteady magnetohydrodynamic (MHD) boundary layer flow of a rotating viscoelastic fluid over an infinite vertical porous plate embedded in a uniform porous medium. Considering the impact of partial velocity slip at the sheet-fluid interface, Seth et al. [5] have focused on the two-dimensional hydromagnetic, natural convective flow of an electrically conducting, incompressible, and viscoelastic fluid past a vertically upward, nonlinearly stretching sheet.

Shahzadi and Bilal [6] talked on the effects of permeability on blood flow by using the example of a hybrid nanofluid passing through a bifurcated stenosed artery. By using Carbon Nanotubes (CNTs) suspended in human blood/water as the base fluid on a stretched sheet, Alkasasbeh et al. [7] wanted to study the features of heat transfer and magnetohydrodynamics (MHD) Casson nanofluid at the existence of free convection boundary layer flow. Casson nanofluid, which is employed as a lubricant, was examined by Archana et al. [8] in the incompressible and compressed flow between two parallel plates. In a two-layer Casson model with blood serving as the base fluid in both levels, one layer is filled with TiO_2, while the second layer includes both TiO_2 and Graphene, Amin et al. [9] looked into the mass and energy transmission. Recent studies have investigated nanofluid flow and

heat transfer in Couette-driven channels with embedded cavities using Buongiorno's model. Rossi di Schio et al. [10] examined the influence of Brownian motion, thermophoresis, and key dimensionless parameters on velocity, temperature, concentration, and Nusselt number. Complementing this, Mokhefi and Rossi di Schio [11] analyzed the effect of magnetic fields, showing how Hartmann number and field inclination significantly alter transport and heat exchange characteristics. Together, these works provide valuable insights into nanofluid convection with and without magnetohydrodynamic effects several very recent works apply Casson-type models with hybrid or mono-nanoparticles to arterial and channel flows, demonstrating practical relevance to biomedical problems: Nazeer et al. [12] analysed entropy generation and heat transfer in blood-gold Casson nanofluids in wavy channels with clinical applications in skin therapies, while Khanduri and Sharma [13] examined Hall and ion slip effects for Au-GO/blood suspensions in catheterized stenosed arteries. Two-layer and hybrid Casson nanofluid formulations further illustrate how nanoparticle choice (e.g., TiO_2, Graphene, Au) and layering can alter mass/heat transport in physiologically relevant geometries results that can inform hyperthermia, enhanced heat removal, and nanoparticle-assisted drug transport strategies. Motivation of this study comes from the listed reference works, applications from industrial difficulties, and the primary interest in learning about the effects of radiation-absorption and Hall and ion slip condition. Casson nanofluid is taken into consideration in this work. For the closed form solution of the non-dimensional governing equations, the analytical approach is used.

2. Mathematical Formulation

Flow description of the present problem is shown in Figure 1. Consider the Hall and ion slip effects, unsteady, fully developed flow of viscous incompressible and electrically conducting Casson fluid in a region between two vertical channel walls situated at $z' = 0$ and $z' = h' = d + a\sin\lambda x'$, respectively. The following equations govern the flow field (Amin et al. [9], Bunonyo et al. [14] and Babu et al. [15]):

(i) The uniform magnetic field is applied perpendicularly to the direction of the nanofluid flow.

(ii) With regard to the *z*-axis, the system is rotated.

(iii) It is considered that nano-particles are consistent in size and shape.

(iv) Nanoparticles in the fluid phase are both in a condition of thermal equilibrium.

(v) Since the plate has an unlimited surface area, the only physical variables that depend on *z* and *t* are pressure and temperature.

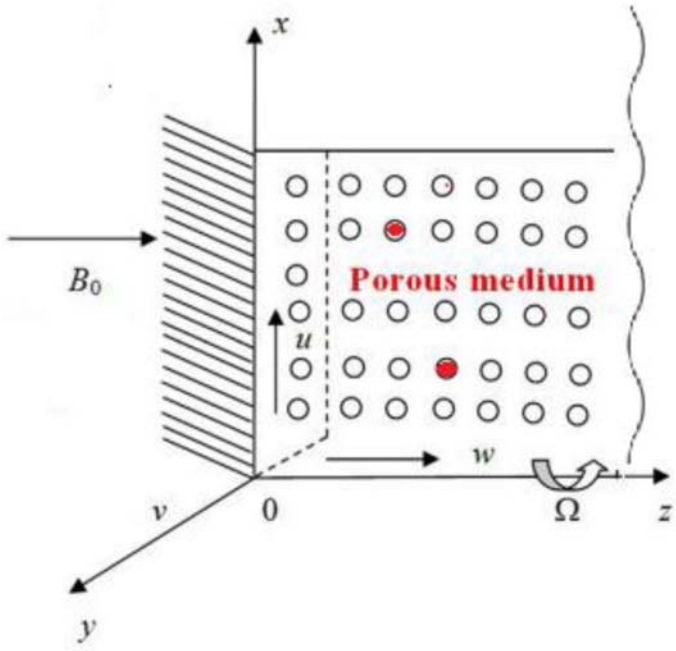

Figure 1. Physical model of the problem.

The governing equation incorporating continuity, momentum and energy equations in the *x* and *z* direction (Vijayakumar and Jancy Rani [16]) is written as

$$\frac{\partial w'}{\partial z'} = 0, \tag{1}$$

$$\rho_{nf}\left(\frac{\partial u'}{\partial t'} + w'\frac{\partial u'}{\partial z'} - 2\Omega v'\right) = \left(1 + \frac{1}{\beta'}\right)\mu_{nf}\frac{\partial^2 u'}{\partial z'^2} + B_0 J_y - \mu_{nf}\frac{u'}{k'} + g(\rho\beta_T)_{nf}(T - T_0), \tag{2}$$

$$\rho_{nf}\left(\frac{\partial v'}{\partial t'} + w'\frac{\partial v'}{\partial z'} - 2\Omega u'\right) = \left(1 + \frac{1}{\beta'}\right)\mu_{nf}\frac{\partial^2 v'}{\partial z'^2} - B_0 J_z - \mu_{nf}\frac{v'}{k'}, \tag{3}$$

$$(\rho c_p)_{nf}\left(\frac{\partial T}{\partial t'} + w'\frac{\partial T}{\partial z'}\right) = k_{nf}\frac{\partial^2 T}{\partial z'^2} - \frac{\partial q_r}{\partial z'} - Q_T(T - T_0). \tag{4}$$

The boundary conditions are stated as

$$t > 0,\ u' = \frac{\sqrt{k_p}}{\alpha_f}\frac{\partial u'}{\partial z'},\ v' = 0,\ T = T_1 + \varepsilon e^{i\omega t}(T_0 - T_1) \text{ at } z = 0,$$

$$u' = -\frac{\sqrt{k_p}}{\alpha_f}\frac{\partial u'}{\partial z'},\quad v' = 0,\quad T = T_1 \text{ at } z = h. \tag{5}$$

We consider the solution of equation (1) as

$$w = -W_0, \tag{6}$$

where the constant $-W_0$ denotes the negative for blowing injection $(W_0 < 0)$ and the normal velocity at the plate which is positive suction $(W_0 > 0)$. Following Rosseland approximation (Ali et al. [17], Ahmed et al. [18] and Alkuhayli [19]), the radiative heat flux q_r, is modeled as

$$q_r = -\frac{4\sigma'}{3k_2}\frac{\partial T^4}{\partial z'}. \tag{7}$$

Considering that the flow is surrounded by a temperature different, then the linear combination of temperature T^4 is defined. We expand T^4 by Taylor series about T_∞ as follows:

$$T^4 = T_\infty^4 + 4T_\infty^3(T - T_\infty) + 6T_\infty^3(T - T_\infty)^2 + \cdots. \tag{8}$$

Ignoring higher order expressions forward to the foremost degree within

$$T^4 \approx -3T_\infty^4 + 4T_\infty^3 T \tag{9}$$

with respect to z, differentiate the equation (7) and making use the equation (9)

$$\frac{\partial q_r}{\partial z'} = -\frac{16T_\infty^4}{3k_2}\frac{\partial T^4}{\partial z^2}. \tag{10}$$

The electron-atom collision frequency is considered to be extremely high, therefore Hall and ion slip currents cannot be ignored. As a result, the Hall and ion slip currents generate velocity in the y direction. When the magnetic field is sufficiently strong, the generalised Ohm's equation is modified to incorporate the Hall and ion slip effect as Vijayakumar and Jancy Rani [16]:

$$J = \sigma'(E + q \times B) - \frac{\omega_e \tau_e}{B_0}(J \times B) + \frac{\omega_e \tau_e \alpha_i}{B_0^2}((J \times B) \times B), \tag{11}$$

where q, B, E, J, σ', α_i are respectively the velocity vector, the magnetic field vector, the electric field vector, the current density vector, the effective electric conductivity of hybrid blood and Hall parameter.

The Maxwell equations are

$$\nabla \times E = -\frac{\partial B}{\partial t}, \quad \nabla \cdot B = 0, \quad \nabla \cdot J = 0. \tag{12}$$

Further it is assumed that $\omega_e \tau_e \sim O(1)$ and $\omega_e \tau_e << 1$, in equation (11), the electron pressure gradient and thermoelectric effects are neglected, i.e., the electric field $E = 0$ under these assumption, equation (11) reduces to

$$(1 + \alpha_i \alpha_e) J_x + \alpha_e J_z = \sigma' B_0 v, \tag{13}$$

$$(1 + \alpha_i \alpha_e) J_z - \alpha_e J_x = -\sigma' B_0 u. \tag{14}$$

We get by solving equations (13) and (14):

$$J_x = \sigma' B_0 (\beta_{II} u + \beta_I v), \tag{15}$$

$$J_z = -\sigma' B_0(\beta_{II} v - \beta_I u). \tag{16}$$

Substituting equations (15) and (16) into (2) and (3), we obtain

$$\frac{\partial u'}{\partial t'} + w' \frac{\partial u'}{\partial z'} - 2\Omega v' = \left(1 + \frac{1}{\beta'}\right) \frac{\mu_{nf}}{\rho_{nf}} \frac{\partial^2 u'}{\partial z'^2} + \frac{\sigma' B_0^2 (\beta_I v - \beta_{II} u)}{\rho_{nf}}$$

$$- \frac{\mu_{nf}}{\rho_{nf}} \frac{u'}{k'} + g(\rho\beta)_{nf} (T - T_0) \cos(\phi), \tag{17}$$

$$\frac{\partial v'}{\partial t'} + w' \frac{\partial v'}{\partial z'} - 2\Omega u' = \left(1 + \frac{1}{\beta'}\right) \frac{\mu_{nf}}{\rho_{nf}} \frac{\partial^2 v'}{\partial z'^2} - \frac{\sigma' B_0^2 (\beta_{II} u + \beta_I v)}{\rho_{nf}} - \frac{\mu_{nf}}{\rho_{nf}} \frac{v'}{k'}, \tag{18}$$

where

$$\beta_I = \frac{1 + \alpha_e \alpha_i}{(1 + \alpha_e \alpha_i)^2 + \alpha_e^2}, \quad \beta_{II} = \frac{\alpha_e}{(1 + \alpha_e \alpha_i)^2 + \alpha_e^2}.$$

Combining equations (17) and (18), let $q' = u' + iv'$,

$$\frac{\partial q'}{\partial t'} + w' \frac{\partial q'}{\partial z'} - 2\Omega q' = \left(1 + \frac{1}{\beta'}\right) \frac{\mu_{nf}}{\rho_{nf}} \frac{\partial^2 q'}{\partial z'^2} - \frac{\sigma' B_0^2 (\beta_I + i\beta_{II}) q'}{\rho_{nf}}$$

$$- \frac{\mu_{nf}}{\rho_{nf}} \frac{q'}{k'} + g(\rho\beta)_{nf} (T - T_0) \cos(\phi). \tag{19}$$

The boundary conditions are stated as

$$t > 0,\ q' = \frac{\sqrt{k_p}}{\alpha_f} \frac{\partial q'}{\partial z'},\ v' = 0,\ T = T_1 + \varepsilon e^{i\omega t} (T_0 - T_1) \text{ at } z = 0, \tag{20}$$

$$q' = -\frac{\sqrt{k_p}}{\alpha_f} \frac{\partial q'}{\partial z'},\ v' = 0,\ T = T_1 \text{ at } z = h. \tag{21}$$

Now, we introduce the following dimensionless parameters:

$$q = \frac{q'}{q_0}, \quad z = \frac{z'}{d}, \quad h = \frac{h'}{d}, \quad t = \frac{t' q_0}{h}, \quad \theta = \frac{T - T_0}{T_1 - T_0},$$

with the boundary conditions, the equations (19)-(21) and (4) obtained using dimensionless variables are

$$a_1 Re \frac{\partial q}{\partial t} - S\, Re a_1 \frac{\partial q}{\partial z} = a_2 \left(1 + \frac{1}{\beta'}\right) \frac{\partial^2 q}{\partial z^2} - s_1 q + a_5 Gr\, \theta\, Cos\, \phi, \tag{22}$$

$$PrRe\left(a_5 \frac{\partial \theta}{\partial t} - S \frac{\partial \theta}{\partial z}\right) = \left(a_6 + \frac{4}{3} Rd\right) \frac{\partial^2 \theta}{\partial z^2} - Q\theta, \tag{23}$$

with the boundary conditions

$$\frac{\partial q}{\partial z} = \alpha_f \sigma q, \quad \theta = 1 + \varepsilon e^{i\omega t} \text{ at } z = 0, \tag{24}$$

$$\frac{\partial q}{\partial z} = -\alpha_f \sigma q, \quad \theta = 1 \text{ at } z = h. \tag{25}$$

Here $Re = \frac{q_0 d}{\gamma_f}$ is the Reynolds number, $S = \frac{w_0}{U_0}$ is the suction parameter, $R = \frac{2i\Omega d}{q_0}$ is the Rotation parameter, $\sigma = \frac{d}{\sqrt{k'}}$ is the Porous parameter, $Q = \frac{Q_T d^2}{k_f}$ is the Heat source parameter, $Rd = \frac{4\sigma' T_0^3}{k' k_f}$ is the Radiation parameter and $Pr = \frac{(\rho c_p)_f \gamma_f}{k_f}$ is the Prandtl number.

Table 1. Thermophysical properties of base fluid and nanoparticles

Physical property	Blood	Gold
ρ (KGM^{-3})	1063	19320
K (W/mK)	0.492	314
C_p (J/kgK)	3591	129
σ (Sm^{-1})	6.67×10^{-1}	4.10×10^{7}
β (k^{-1})	0.18×10^{-5}	1.4×10^{-5}

As a function of the nanoparticle, the following definitions for effective density, effective dynamic viscosity, thermal expansion coefficient, thermal

conductivity, and electrical conductivity (see Krishna and Chamkha [20]) are given, respectively:

$$(\rho)_{nf} = (1-\phi')\rho_f + \phi\rho_s,$$

$$\mu_{nf} = \frac{\mu_f}{(1-\phi')^{2.5}}, (\rho\beta)_{nf} = (1-\phi')(\rho\beta)_f + \phi'(\rho\beta)_s,$$

$$K_{nf} = K_f\left(\frac{(K_s+2K_f)-2\phi'(K_f-K_s)}{(K_s+2K_f)+2\phi'(K_f-K_s)}\right),$$

$$\sigma_{nf} = \sigma_f\left(\frac{(\sigma_n+2\sigma_f)-2\phi'(\sigma_f-\sigma_n)}{(\sigma_n+2\sigma_f)+2\phi'(\sigma_f-\sigma_n)}\right),$$

where ϕ' is the volume of the nanoparticles that are made of solid material, ρ_f and ρ_s are the densities of the fluid and solid particles, β_s and β_f are the coefficients of thermal expansion of the solid and fluid, K_f and K_s are the thermal conductivity of the base fluid and the solid, σ_f is the electrical conductivity of the fluid, respectively.

3. Method of Solution

Equations (22)-(25) constitute nonlinear partial differential equations with complex closed-form solutions. To solve these equations by transforming them into ordinary differential equations, the unsteady flow is imposed on the mean steady flow. In the vicinity of the plate, the formulas for velocity, temperature, and concentration are assumed $(\varepsilon < 1)$, as follows:

$$q = q_0 + \varepsilon e^{i\omega t} q_0 + O(\varepsilon^2), \tag{26}$$

$$\theta = \theta_0 + \varepsilon e^{i\omega t}\theta_0 + O(\varepsilon^2). \tag{27}$$

Equations (22)-(25) are simplified by applying equations (26)-(27) and equating the harmonic and non-harmonic terms, and neglecting the higher

order of $O(\varepsilon^2)$, and simplifying to get the following pairs of equations for q_0, θ_0 and q_1, θ_1,

$$\frac{\partial^2 q_0}{\partial z^2} + S_6 \frac{\partial q_0}{\partial z} - S_{88}\theta_0 = S_8\theta_0, \tag{28}$$

$$\frac{\partial^2 \theta_0}{\partial z^2} + S_3 \frac{\partial \theta_0}{\partial z} - S_5\theta_0 = 0, \tag{29}$$

$$\frac{\partial^2 q_1}{\partial z^2} + S_6 \frac{\partial q_1}{\partial z} - S_7\theta_1 = S_8\theta_1, \tag{30}$$

$$\frac{\partial^2 \theta_1}{\partial z^2} + S_3 \frac{\partial \theta_1}{\partial z} - S_4\theta_1 = 0. \tag{31}$$

Subject to the boundary conditions

$$\frac{\partial q_0}{\partial z} = \alpha_f \sigma q_0, \ \theta_0 = 1 \text{ at } z = 0, \tag{32}$$

$$= -\alpha_f \sigma q_0, \ \theta_0 = 1 \text{ at } z = h, \tag{33}$$

$$\frac{\partial q_1}{\partial z} = \alpha_f \sigma q_1, \ \theta_1 = 1 \text{ at } z = 0, \tag{34}$$

$$= -\alpha_f \sigma q_1, \ \theta_1 = 1 \text{ at } z = h. \tag{35}$$

Solving the equations (28)-(31) with respect to the boundary conditions (32)-(35), we obtain the solutions of velocity and temperature as follows:

$$q = A_5 e^{m_5 z} + A_6 e^{m_6 z} + S_9 e^{m_1 z} + S_{10} e^{m_2 z} + \varepsilon e^{i\omega t}(A_7 e^{m_7 z} + A_8 e^{m_8 z} + S_{11} e^{m_3 z} + S_{12} e^{m_4 z}), \tag{36}$$

$$\theta(z, t) = A_1 e^{m_1 z} + A_2 e^{m_2 z} + \varepsilon e^{i\omega t}(A_3 e^{m_3 z} + A_4 e^{m_4 z}). \tag{37}$$

At the surface of the plate $z = 0, h$. Skin friction and Nusselt number are defined in non-dimensional form as follows:

$$\tau = \frac{\partial q}{\partial z} \text{ at } z = 0, h,$$

$$Nu = -\frac{\partial \theta}{\partial z} \text{ at } z = 0, h.$$

4. Results and Discussions

The governing equations along with the relevant physical conditions are solved by employing a perturbation technique. The effects of the governing parameters on the velocity and temperature distributions are analyzed and illustrated graphically in Figures 2-16 for representative parameter values using MATHEMATICA 12.0.

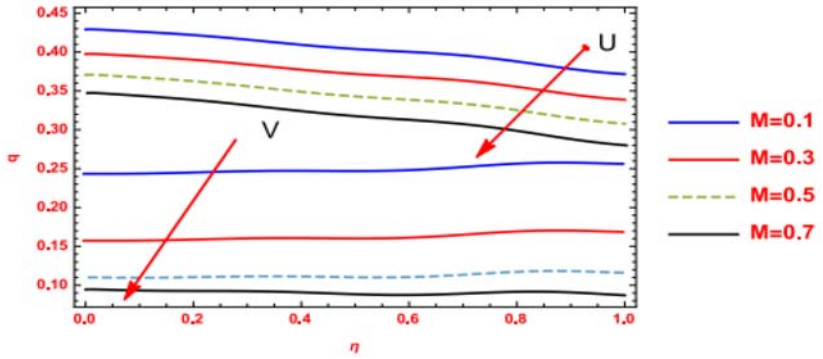

Figure 2. Velocity profile for varying *M*.

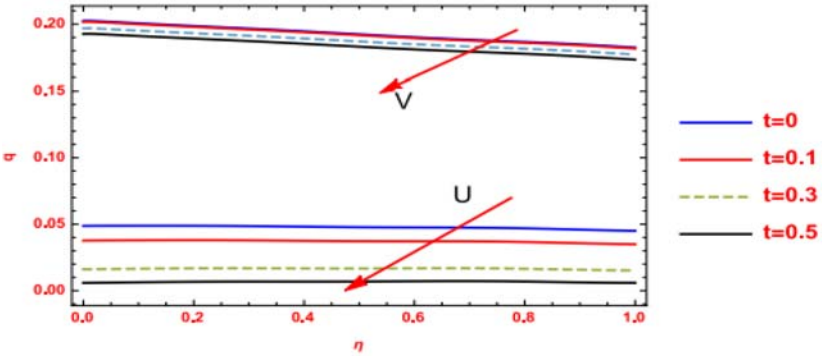

Figure 3. Velocity profile for varying *t*.

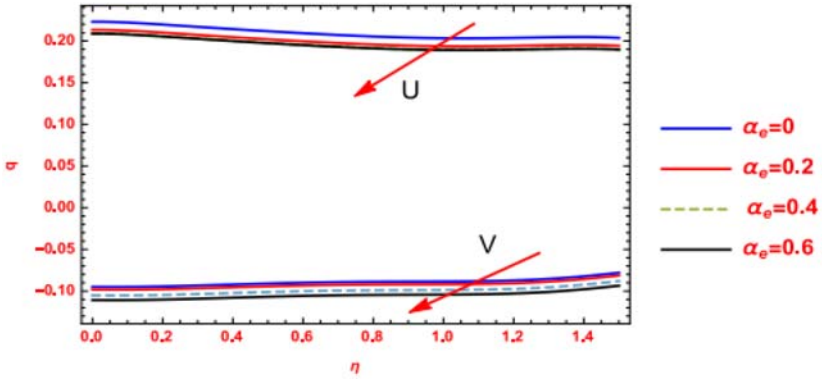

Figure 4. Velocity profile for varying α_e.

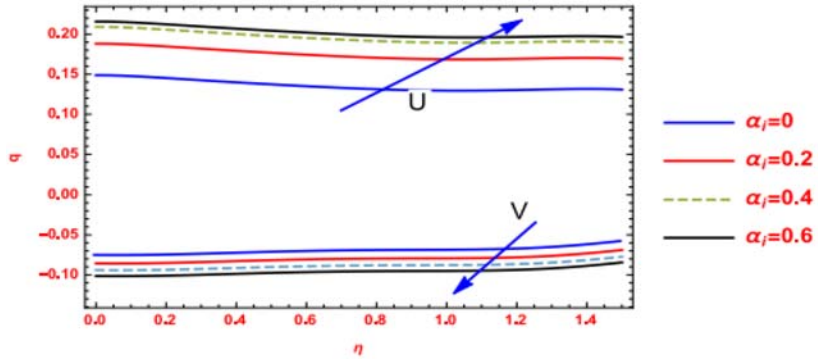

Figure 5. Velocity profile for varying α_i.

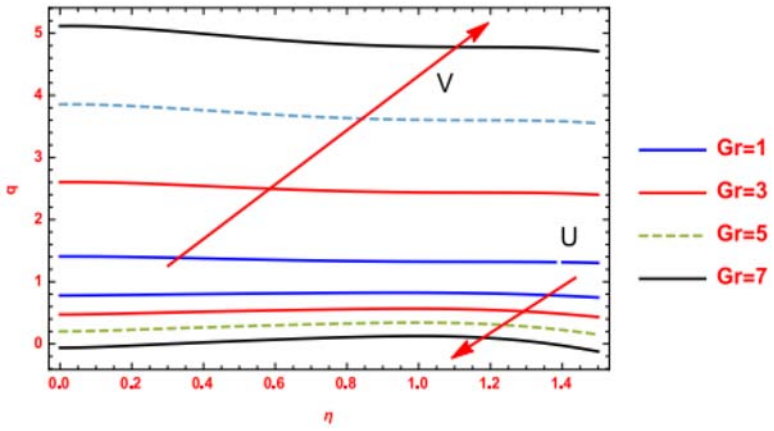

Figure 6. Velocity profile for varying *Gr*.

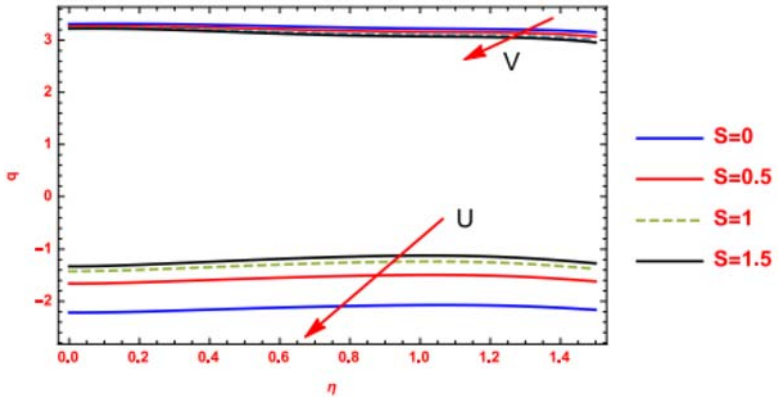

Figure 7. Velocity profile for varying *S*.

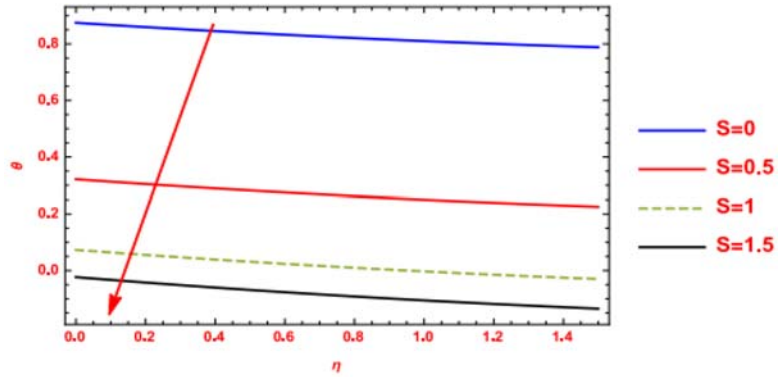

Figure 8. Temperature profile for varying *S*.

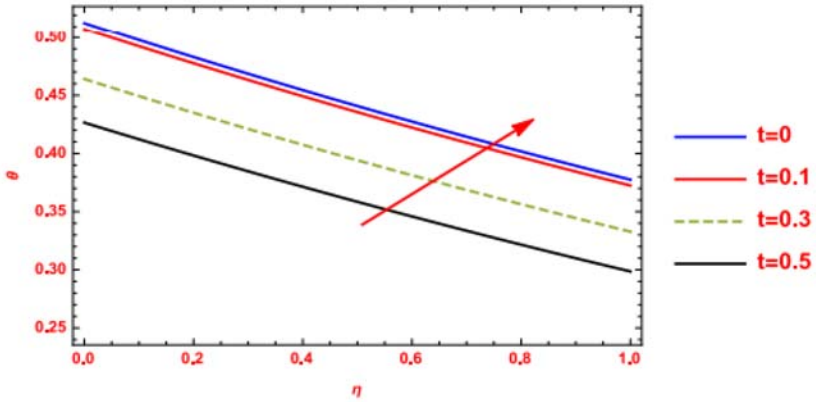

Figure 9. Temperature profile for varying *t*.

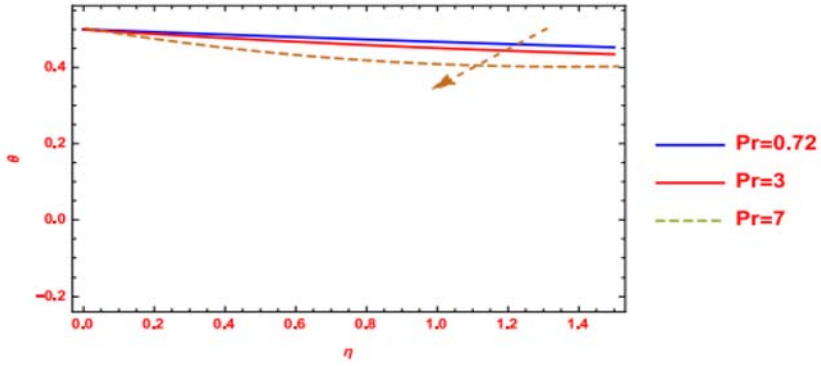

Figure 10. Temperature profile for varying *Pr*.

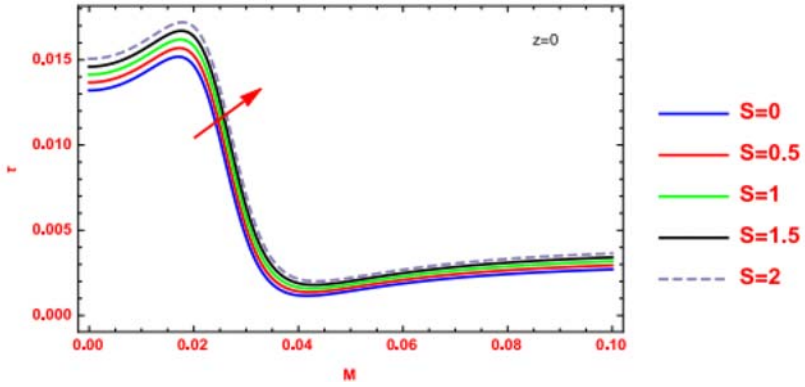

Figure 11. Skin friction for varying *S* at $z = 0$.

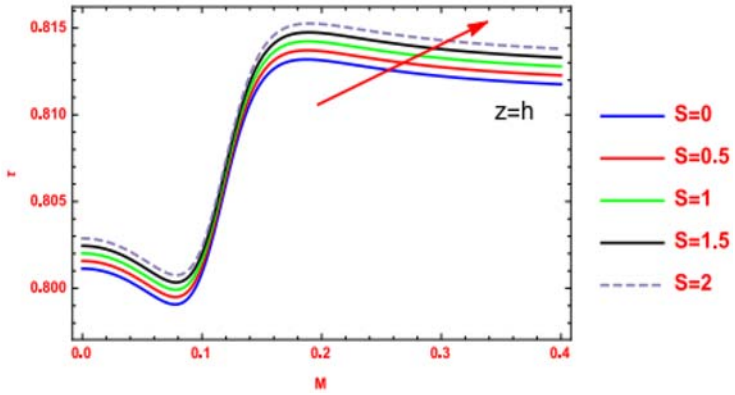

Figure 12. Skin friction for varying *S* at $z = h$.

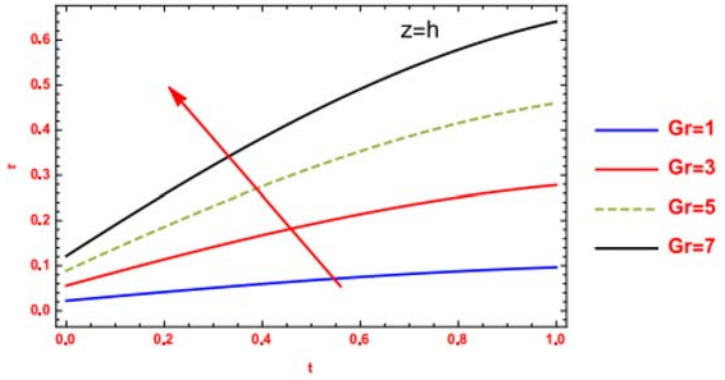

Figure 13. Skin friction for varying *Gr* at $z = h$.

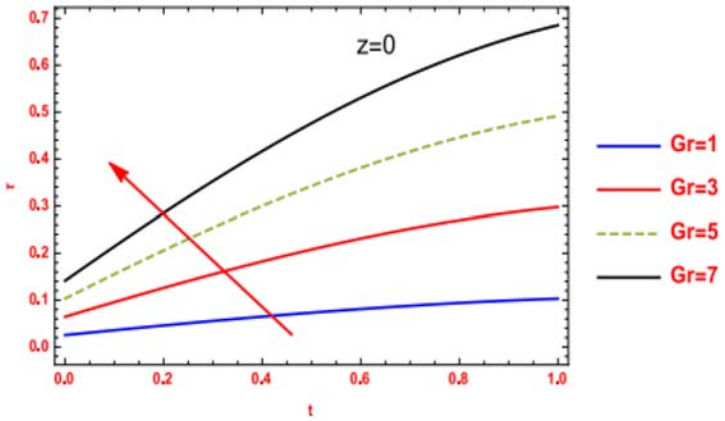

Figure 14. Skin friction for varying *Gr* at $z = 0$.

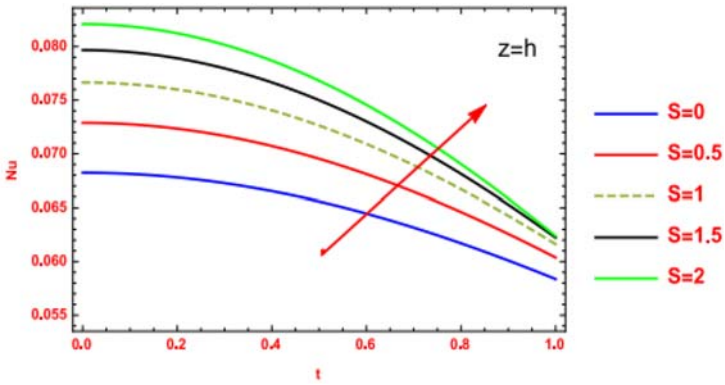

Figure 15. Nusselt number for varying *S* at $z = h$.

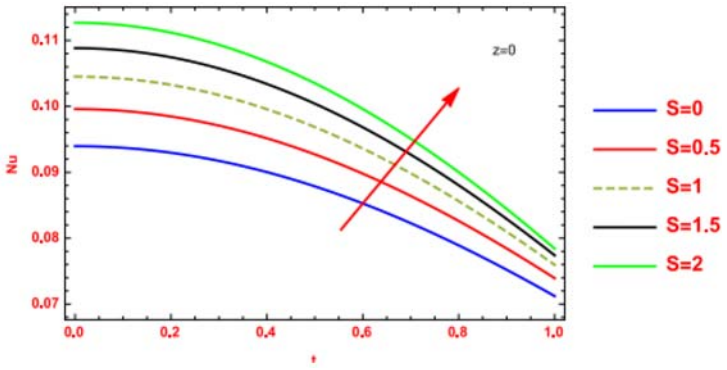

Figure 16. Nusselt number for varying S at $z = 0$.

Figure 2 displays Hartmann number (M) the behavior of velocity profiles in the presence of a magnetic field can depend on various factors, including the fluid properties (conductivity, viscosity), the strength and orientation of the magnetic field, and the geometry of the flow. Additionally, the presence of nanoparticles in a nanofluid can further complicate the behavior of the fluid, as nanoparticle properties also influence the response to the magnetic field. Hence, increasing values of the Hartmann number (M) lead to the suppression of fluid motion and can result in altered velocity profiles in both the U and V velocities, especially in magnetohydrodynamic flows of regular and nanofluids. Figure 3 illustrates the effect of time on the velocity distribution in the blood-based nanofluid. As time increases, the velocity profiles exhibit oscillatory and gradually attenuated behavior due to the pulsatile nature of blood flow combined with the sinusoidal channel geometry. The presence of wavy walls introduces periodic flow disturbances, leading to time-dependent variations in velocity. In the constricted regions of the channel, the fluid accelerates, whereas in the wider sections, the flow decelerates, resulting in a dynamically varying velocity profile. Figure 4 depicts the influence of the Hall parameter (α_e), on the velocity field. The observed behavior is attributed to the action of the Lorentz force arising from the interaction between the applied magnetic field and the electrically conducting fluid. At higher Hall parameter values, the Lorentz force acts perpendicular to both the magnetic field and the primary flow direction,

which reduces the axial velocity component. Simultaneously, this force induces transverse motion, leading to an enhancement of the velocity component in the V direction.

Figure 5 shows as the ion slip parameter (α), increases, it signifies that there is a greater relative motion or slip between the ions and the nanoparticles in the nanofluid. This increased slip can lead to changes in the velocity profile. Typically, this would observe that the fluid velocity U decreases because the presence of nanoparticles may introduce additional resistance to hinder the flow of the fluid. The velocity component V perpendicular to the flow direction might increase because of these changes in the flow dynamics.

Figure 6 shows the higher thermal Grashof numbers (Gr) that can lead to more turbulent flow patterns, especially in nanofluids where nanoparticles may introduce additional mixing mechanisms. Turbulence can further increase the complexity of the velocity profiles, leading to increase velocities in V direction. The horizontal velocity component U may decrease to remain relatively constant, depending on the specific conditions of the problem. In the case of nanofluids, nanoparticles can enhance heat transfer due to their high thermal conductivity. As the Grashof number (Gr) increases, the convective heat transfer also increases, which can affect the temperature distribution and consequently, the velocity profile.

Figure 7 illustrates the effect of the suction parameter S on the velocity components U (axial) and V (transverse) for both regular fluids and nanofluids. It is observed that increasing values of S lead to a reduction in velocities in both directions. This behavior is attributed to the enhanced suction at the channel walls, which draws fluid toward the surface and reduces the momentum boundary layer thickness. In the case of nanofluids, the presence of suspended nanoparticles further increases the effective drag within the flow. Consequently, stronger suction suppresses fluid motion and results in a significant decrease in both velocity components. Figure 8

demonstrates that increasing values of the suction parameter lead to a noticeable reduction in the temperature profile of the nanofluid, particularly in the case of blood-based fluids. This behavior is attributed to the enhanced removal of fluid particles near the surface, which effectively reduces the thermal boundary layer thickness. As suction intensifies, it promotes rapid extraction of thermal energy from the fluid, thereby lowering the local temperature. Additionally, increased suction suppresses convective currents within the boundary layer, limiting heat transport and reinforcing the cooling effect. These findings are consistent with prior studies, such as those reported by Khan and Pop [21], who observed similar thermal boundary layer behavior in nanofluids under varying suction conditions. This mechanism has significant implications for biomedical heat regulation, especially in applications involving targeted drug delivery and localized thermal therapies.

Figure 9 reveals that as time progresses, the temperature of the nanofluid (blood fluid) increases along the z direction. This behavior is due to the continuous application of thermal energy and the gradual diffusion of heat throughout the fluid domain. Over time, the thermal boundary layer expands radially, allowing more heat to penetrate into the nanofluid. The nanoparticles within the blood fluid enhance thermal conductivity, contributing to the overall temperature rise. Similar observations were reported by Nadeem et al. [22], where time-dependent nanofluid flows exhibited increasing thermal response due to sustained energy input and enhanced nanoparticle interaction. Figure 10 indicates that an increase in the Prandtl number leads to a decline in temperature along the z direction in blood-based nanofluids. A higher Prandtl number implies lower thermal diffusivity, which restricts heat conduction and results in a thinner thermal boundary layer. Consequently, less heat is transferred away from the surface, causing the temperature to decrease with radial distance. These results are in good agreement with those reported by Khan and Pop [21], who observed a similar reduction in temperature profiles for nanofluids with higher Prandtl numbers. The numerical results, as shown in Figures 11 and 12, indicate that

increasing the suction parameter significantly enhances the skin friction coefficients at both the upper and lower wavy walls in blood-based nanofluid flow. This is because higher suction rates draw fluid toward the walls, reducing boundary layer thickness and intensifying the near-wall velocity gradients. As a result, wall shear stress increases. Similar observations were reported by Nadeem et al. [22], who noted that stronger suction enhances skin friction in boundary-layer nanofluid flows. The results clearly demonstrate that increasing the Grashof number increases the skin friction on both the upper and lower wavy walls in blood-based nanofluid flow. This behavior is primarily due to the strengthening of buoyancy forces, which enhances the convection process. With higher Grashof numbers, the induced convective currents near the wall become more vigorous, leading to an increase in the velocity gradient and, consequently, in skin friction.

Figures 13 and 14 show that skin friction increases when the Grashof number rises at both the upper $(z = h)$ and lower $(z = 0)$ wavy walls in nanofluid (blood fluid) flow. This is due to the enhancement of buoyancy driven forces, which intensify natural convection and fluid motion near the walls. The stronger velocity gradients near the wavy boundaries increase the shear stress, leading to higher skin friction. Figures 15 and 16 demonstrate that an increase in the suction parameter leads to a higher Nusselt number at both the upper $(z = h)$ and lower $(z = 0)$ wavy walls in nanofluid (blood fluid) flow. This is due to the enhanced heat transfer caused by the reduction in thermal boundary layer thickness from the suction effect. The presence of nanoparticles in the blood fluid further improves thermal conductivity, enhancing the overall heat transfer.

5. Conclusion

The present analysis investigates the effects of Hall and ion slip currents on unsteady MHD free convective rotating flow of a Casson nanofluid through a porous sinusoidal channel. The key findings of the study are summarized as follows:

(i) The fluid velocity decreases with increasing Hartmann number, time, and thermal Grashof number due to enhanced magnetic and buoyancy resistance.

(ii) An increase in the Hall parameter reduces the axial velocity, while ion slip effects exhibit an opposing influence on the flow behavior.

(iii) Fluid temperature decreases with increasing suction parameter and Prandtl number, indicating effective thermal boundary layer control.

(iv) Skin friction coefficients increase at both wavy walls with higher suction and Grashof numbers.

(v) The Nusselt number is enhanced with suction, demonstrating improved heat transfer characteristics of the Casson nanofluid.

Acknowledgement

The authors thank the anonymous referees for their valuable suggestions and constructive criticisms which improved the presentation of the paper.

Appendix

This section provides supplementary mathematical derivations and extended formulations that support the governing equations and analytical solutions discussed in the main text. These details are included to ensure completeness and reproducibility of the analysis of unsteady MHD Casson nanofluid flow through a porous sinusoidal artery channel under the influence of a magnetic field,

$$a_1 = \frac{\rho_{nf}}{\rho_f},\ a_2 = \frac{\mu_{nf}}{\mu_f},\ a_3 = \frac{\sigma_{nf}}{\sigma_f},\ a_4 = \frac{(\rho\beta)_{nf}}{(\rho\beta)_f},\ a_5 = \frac{(\rho c_p)_{nf}}{(\rho c_p)_f},\ a_6 = \frac{k_{nf}}{k_f},$$

$$s_1 = a_3 M^2(\beta_{II} + i\beta_I) - 2ia_1 R + a_4\sigma^2,\ s_2 = a_6\frac{4}{3}Rd,$$

$$s_3 = \frac{RePrS}{s_2},\ s_4 = \frac{Q + RePra_5}{s_2},\ s_5 = \frac{Q_0}{s_2},\ s_6 = \frac{SRea_1}{a_2},$$

$$s_7 = \frac{s_1(Rei\omega + 1)}{a_2},\ s_{88} = \frac{s_1}{a_2},\ s_8 = \frac{s_5 Gr\cos(\phi)}{a_2},\ s_9 = \frac{s_8 A_1}{m_1^2 + s_1 m_1 - s_8},$$

$$s_{10} = \frac{s_2 A_2}{m_2^2 + s_6 m_2 - s_8},\ s_{11} = \frac{s_8 A_3}{m_3^2 + s_6 m_2 - s_8},\ s_{12} = \frac{s_8 A_4}{m_3^2 + s_6 m_2 - s_7},$$

$$s_{13} = m_5\alpha_f\sigma,\ s_{14} = m_6\alpha_f\sigma,\ s_{15} = \alpha_f\sigma(s_9 + s_{10}) - (s_9 m_1 + s_{10} m_2),$$

$$M^2 = \frac{d^2\sigma_f B_0^2}{\mu_f},\ m_1 = \frac{-s_3 + \sqrt{s_3^2 + 4s_5}}{2},\ m_2 = \frac{-s_3 - \sqrt{s_3^2 + 4s_5}}{2},$$

$$m_3 = \frac{-s_3 + \sqrt{s_3^2 + 4s_4}}{2},\ m_4 = \frac{-s_3 - \sqrt{s_3^2 + 4s_4}}{2},$$

$$m_5 = \frac{-s_6 + \sqrt{s_6^2 + 4s_{88}}}{2},\ m_6 = \frac{-s_6 - \sqrt{s_6^2 + 4s_{88}}}{2},$$

$$m_7 = \frac{-s_6 + \sqrt{s_6^2 + 4s_7}}{2},\ m_8 = \frac{-s_6 - \sqrt{s_6^2 + 4s_7}}{2},$$

$$A_1 = -1 + A_2,\ A_2 = \frac{e^{m_1 h} - 1}{e^{m_1 h} - e^{m_2 h}},\ A_3 = \frac{e^{m_3 h} - e^{m_4 h}}{e^{m_3 h}},\ A_4 = 1 - A_3,$$

$$A_5 = \frac{s_{18} - s_{17}A_6}{s_{16}},\ A_6 = \frac{s_{16}s_{15} - s_{13}s_{18}}{s_{14}s_{16} - s_{13}s_{17}},\ A_8 = \frac{s_{23}s_{19} - s_{20}s_{22}}{s_{23}s_{21} - s_{20}s_{24}}.$$

References

[1] A. Afsar Khan, R. Ellahi and K. Vafai, Peristaltic transport of a Jeffrey fluid with variable viscosity through a porous medium in an asymmetric channel, Advances in Mathematical Physics 2012 (2012), 1-15. https://doi.org/10.1155/2012/169642.

[2] L. Parasuraman, N. C. Peddisetty and G. Periyannagounder, Radiation effects on an unsteady MHD natural convective flow of a nanofluid past a vertical plate, Thermal Science 19(3) (2015), 1037-1050. https://doi.org/10.2298/TSCI121208155P.

[3] J. K. Singh, S. G. Begum and G. S. Seth, Influence of Hall current and wall conductivity on hydromagnetic mixed convective flow in a rotating Darcian channel, Physics of Fluids 30(11) (2018), 113602. https://doi.org/10.1063/1.5054654.

[4] Jitendra Kumar Singh, G. S. Seth and Begum, Unsteady MHD natural convection flow of a rotating viscoelastic fluid over an infinite vertical porous plate due to oscillating free-stream, Multidiscipline Modeling in Materials and Structures 14(2) (2018), 236-260. https://doi.org/10.1108/MMMS-06-2017-0054.

[5] G. S. Seth, A. Bhattacharyya, R. Kumar and A. J. Chamkha, Entropy generation in hydromagnetic nanofluid flow over a non-linear stretching sheet with Naviers velocity slip and convective heat transfer, Physics of Fluids 30(12) (2018), 122003. https://doi.org/10.1063/1.5054099.

[6] I. Shahzadi and S. Bilal, A significant role of permeability on blood flow for hybrid nanofluid through bifurcated stenosed artery: Drug delivery application, Computer Methods and Programs in Biomedicine 187 (2020), 105248. https://doi.org/10.1016/j.cmpb.2019.105248.

[7] H. T. Alkasasbeh, M. Z. Swalmeh, H. G. Bani Saeed, F. M. Al Faqih and A. G. Talafha, Investigation on CNTs-water and human blood based Casson nanofluid flow over a stretching sheet under impact of magnetic field, Frontiers in Heat and Mass Transfer 14 (2020), 1-7. https://doi.org/10.5098/hmt.14.15.

[8] M. Archana, M. M. Praveena, K. G. Kumar, S. A. Shehzad and M. Ahmad, Unsteady squeezed Casson nanofluid flow by considering the slip condition and time-dependent magnetic field, Heat Transfer 49(8) (2020), 4907-4922. https://doi.org/10.1002/htj.21859.

[9] A. Amin, S. Munir and U. Farooq, Flow dynamics and convective transport analysis of two-layered dissipative Casson hybrid nanofluid flow in a vertical channel, Proceedings of the Institution of Mechanical Engineers, Part C: Journal of Mechanical Engineering Science 238(2) (2023), 1-10. https://doi.org/10.1177/09544062231170753.

[10] E. Rossi di Schio, A. N. Impiombato, A. Mokhefi and C. Biserni, Theoretical and numerical study on Buongiorno's model with a Couette flow of a nanofluid in a channel with an embedded cavity, Applied Sciences 12(15) (2022), 7751. https://doi.org/10.3390/app12157751.

[11] Abderrahim Mokhefi and Eugenia Rossi di Schio, Effect of a magnetic field on the Couette forced convection of a Buongiorno's nanofluid over an embedded cavity, JP Journal of Heat and Mass Transfer 30 (2022), 89-104. http://dx.doi.org/10.17654/0973576322058.

[12] M. Nazeer, M. Irfan, F. Hussain and I. Siddique, Entropy generation analysis in Blood-Gold Casson nanofluid through horizontal wavy channel with velocity and thermal slips: applications in skin diseases, Journal of Computational Biophysics and Chemistry 22(3) (2023), 259-272. https://doi.org/10.1142/S2737416523400021.

[13] U. Khanduri and B. K. Sharma, Hall and ion slip effects on hybrid nanoparticles (Au-GO/blood) flow through a catheterized stenosed artery with thrombosis Proceedings of the Institution of Mechanical Engineers, Part C: Journal of Mechanical Engineering Science 237(10) (2022), 22562278. https://doi.org/10.1177/09544062221136710.

[14] K. W. Bunonyo, E. Amos and C. Nwaigwe, Modeling the treatment effect on LDL-C and atherosclerotic blood flow through microchannel with heat and magnetic field, International Journal of Mathematics Trends and Technology 67(10) (2021), 41-58. https://doi.org/10.14445/22315373/IJMTT-V67I10P504.

[15] B. Hari Babu, P. Srinivasa Rao and S. V. K. Varma, Hall and ion-slip effects on MHD free convection flow of rotating Jeffrey fluid over an infinite vertical porous surface, Heat Transfer 50(2) (2020), 1776-1798. https://doi.org/10.1002/htj.21954.

[16] R. Vijayakumar and A. Jancy Rani, Hall and ion slip influence on unsteady MHD convective rotating flow of non-Newtonian fluid through porous medium with chemical reaction, International Journal of Mechanical Engineering 7(4) (2022), 564-577.

[17] A. Ali, Soma Mitra Banerjee and S. Das, Hall and ion slip current's impact on magneto-sodium alginate hybrid nanoliquid past a moving vertical plate with ramped heating, velocity slip and Darcy effects, Multidiscipline Modeling in Materials and Structures 1 (2020), 65-101. https://doi.org/10.1108/mmms-12-2019-0218.

[18] B. Ahmed, T. Hayat, F. M. Abbas and A. Alsaedi, Mixed convection and thermal radiation effect on MHD peristaltic motion of Powell-Eyring nanofluid, Int. Commun. Heat Mass Tran. 126 (2021), 105320.

[19] Naif Abdulaziz M. Alkuhayli, Heat transfer analysis of a hybrid nanofluid flow on a rotating disk considering thermal radiation effects, Case Studies in Thermal Engineering 49 (2023), 103131. https://doi.org/10.1016/j.csite.2023.103131.

[20] M. V. Krishna and A. J. Chamkha, Hall and ion slip effects on MHD Rotating Boundary layer flow of Nanofluid past an infinite vertical plate, Results in Physics 15(5) (2019), 102652. https://doi.org/10.1016/j.rinp.2019.102652.

[21] W. A. Khan and I. Pop, Boundary-layer flow of a nanofluid past a stretching sheet, Int. J. Heat Mass Transf. 53(11-12) (2010), 2477-2483. https://doi.org/10.1016/j.ijheatmasstransfer.2010.01.032.

[22] S. Nadeem, R. Mehmood and Z. H. Khan, Heat transfer analysis of a Casson nanofluid over a stretching sheet: A numerical study, Alex. Eng. J. 53 (2014), 219-224. https://doi.org/10.1016/j.aej.2013.11.005.